Scaling of decoherence and energy flow in interacting quantum spin systems

Davide Rossini and Ettore Vicari
Dipartimento di Fisica, Università di Pisa and INFN, Largo Pontecorvo 3, 56127 Pisa, Italy

(Received 11 March 2019; published 16 May 2019)

We address the quantum dynamics of a system composed of a qubit globally coupled to a many-body system characterized by short-range interactions. We employ a dynamic finite-size scaling framework to investigate the out-of-equilibrium dynamics arising from the sudden variation (turning on) of the interaction between the qubit and the many-body system, in particular when the latter is in proximity to a quantum first-order or continuous-phase transition. Although the approach is quite general, we consider d-dimensional quantum Ising spin models in the presence of transverse and longitudinal fields as paradigmatic quantum many-body systems. To characterize the out-of-equilibrium dynamics, we focus on a number of quantum-information-oriented properties of the model. Namely, we concentrate on the decoherence features of the qubit, the energy interchange between the qubit and the many-body system during the out-of-equilibrium dynamics, and the work distribution associated with the quench. The scaling behaviors predicted by the dynamic finite-size scaling theory are verified through extensive numerical computations for the one-dimensional Ising model, which reveal a fast convergence to the expected asymptotic behavior with increasing system size.

DOI: 10.1103/PhysRevA.99.052113

I. INTRODUCTION

The recent progress that has been achieved in the control and manipulation of complex systems at the nanoscale has enabled a wealth of unprecedented possibilities aimed at addressing the unitary quantum evolution of many-body objects. These range from the (nearly) adiabatic dynamics induced by a slow change in time of one of the control parameters to the deep out-of-equilibrium dynamics following an abrupt quench in the system [1–3]. In the latter scenario, several fundamental issues have been investigated, including the onset of thermalization at long times, quantum transport, and localization phenomena due to the mutual interplay between disorder and interactions [4–11]. All of them are eventually devoted to characterizing the highly nonlinear response of the system to the drive, where nonequilibrium fluctuation relations may play a pivotal role [12–15].

Closely related to the scenario we are going to focus on in the present paper, we also mention the increasing interest in monitoring the coherent quantum dynamics of mutually coupled systems, with the purpose of addressing energy interchanges or the relative decoherence properties among the various subsystems [16]. This kind of study is relevant both to understand whether quantum mechanics can enhance the efficiency of energy conversion in complex networks [17,18] and to devise novel quantum technologies which are able to optimize energy storage in portions of the whole system [19–23]. We will stress that energy flows are likely to be influenced by the different quantum phases of the system. Moreover, one would expect an enhanced response in proximity to a quantum phase transition, which requires special attention [24].

The aim of this paper is to shed light on this latter issue. To this purpose, we consider the simplest scenario in which to frame such an analysis: a single qubit globally coupled to a d-dimensional quantum Ising spin model in a transverse and a longitudinal field. This spin model acts as a prototypical quantum many-body system since, when varying the intensity of the two external fields, it may undergo both first-order quantum transitions (FOQTs) and continuous quantum transitions (CQTs). The composite setup belongs to the class of so-called central-spin models where one or a few qubits can be globally or locally coupled to the environmental system (see, e.g., Refs. [25–36]). We put forward a quantitative scaling theory which generalizes the results of Ref. [35] focused on the decoherence properties of the qubit, while also carefully addressing the statistics of energy flow between the qubit and the many-body system. Specifically, we employ the finite-size scaling (FSS) framework, which has been shown to be able to predict the behavior of a system in proximity to either a CQT [37] or a FOQT [38], as well as in a dynamic context [39,40], providing the asymptotic large-size scaling in a variety of situations. A substantial part of this work is devoted to a numerical validation of the dynamic FSS predictions through extensive simulations with exact diagonalization techniques, specialized to the one-dimensional case ($d = 1$).

In our setup, the global system is initialized in a state which is a product of pure states of the qubit q and of the quantum Ising system S. The qubit q is then suddenly coupled to all the L^d spins of S such that a nontrivial unitary dynamics sets in. Note that we admit the possibility to have an interaction Hamiltonian which does not commute with the qubit Hamiltonian so that the decoherent effect on the qubit is not only a pure dephasing. We focus on three quantum-information-oriented properties of the model: the decoherence features of q, the statistics of the work distribution associated with the quench, and the statistics of the energy interchange between q and S during the out-of-equilibrium dynamics. We show that such properties develop dynamic FSS behaviors when the system S is close to quantum transitions. In particular,

our numerics for the one-dimensional Ising systems show that the convergence to the dynamic FSS behavior is remarkably fast, which would prompt a careful assessment of the role of criticality in near-future experiments of quantum transport in complex systems with few spins or particles (of the order of 10).

The paper is structured as follows. We start in Sec. II with the definition of the model and all the relevant quantities that will be analyzed. In Sec. III we summarize the derivation of the dynamic FSS framework, which is capable of addressing the dynamics of a quantum many-body system at either FOQTs or CQTs. We also discuss differences which emerge when considering a disordered phase, corresponding to a general normal phase of many-body systems. The dynamic FSS is then specialized to our system of interest in Sec. IV, explicitly discussing the qubit decoherence functions, the work associated with the initial quench, and the dynamics of the qubit-system energy flow. We discuss the details of the FSS behavior at the CQT point, where extensive numerical simulations in support of the theory are presented (Sec. V), and along the FOQT line, where we also consider a two-level reduction of the many-body system (Sec. VI). Finally, Sec. VII is devoted to a summary and perspectives for future work. In the Appendixes we provide some analytic insight into the special case in which the qubit Hamiltonian commutes with the qubit-system interaction term and discuss in more detail some limitations emerging in the two-level approximation at the FOQT.

II. GENERAL SETTING OF THE PROBLEM

A. Model

Let us consider a d-dimensional quantum many-body system S of size L^d, with Hamiltonian

$$H_S(h) = H_c + H_h, \quad H_h = hP, \tag{1}$$

where P is the spatial integral of local operators, such that $[H_c, P] \neq 0$, and the parameter h drives a quantum transition located at $h = 0$. As a paradigm, we will focus on the quantum Ising model on an L^d lattice,

$$H_c = H_{\rm Is} = -J \sum_{\langle \boldsymbol{x},\boldsymbol{y}\rangle} \sigma_{\boldsymbol{x}}^{(3)} \sigma_{\boldsymbol{y}}^{(3)} - g \sum_{\boldsymbol{x}} \sigma_{\boldsymbol{x}}^{(1)}, \tag{2}$$

where $\sigma^{(k)}$ are the Pauli matrices, the first sum is over all bonds connecting nearest-neighbor sites $\langle \boldsymbol{x}, \boldsymbol{y}\rangle$, and the other sum is over all sites. Hereafter we assume that $\hbar = 1$, $J = 1$, the lattice spacing $a = 1$, and $g > 0$. At $g = g_c$ (in one dimension, $g_c = 1$), the model undergoes a CQT belonging to the $(d + 1)$-dimensional Ising universality class [24,41,42], separating a disordered phase ($g > g_c$) from an ordered one ($g < g_c$). The presence of a homogeneous longitudinal external field is taken into account by adding the term

$$hP = -h \sum_{\boldsymbol{x}} \sigma_{\boldsymbol{x}}^{(3)} \tag{3}$$

to the Hamiltonian (2). The field h drives FOQTs along the $h = 0$ line for any $g < g_c$. At the continuous transition $g = g_c$, such a term is one of the relevant perturbations driving the critical behavior, the other one being the transverse field term $(g - g_c) \sum_{\boldsymbol{x}} \sigma_{\boldsymbol{x}}^{(1)}$.

In addition, let us consider a qubit q whose two-level Hamiltonian can be generally written as

$$H_q = \sum_{a=\pm} \epsilon_a |a\rangle\langle a| = \alpha I_2 + \tfrac{1}{2}\Sigma^{(3)}, \tag{4}$$

where I_2 is the 2×2 identity matrix and the Pauli operator $\Sigma^{(3)}$ is associated with the two states $|\pm\rangle$ of the qubit, so $\Sigma^{(3)}|\pm\rangle = \pm|\pm\rangle$. Therefore,

$$\epsilon_\pm = \alpha \pm \tfrac{1}{2}\delta, \quad \delta = \epsilon_+ - \epsilon_-. \tag{5}$$

The qubit is globally and homogeneously coupled to the many-body system S, through the Hamiltonian term

$$H_{qS} = (u\Sigma^{(3)} + v\Sigma^{(1)})P, \tag{6}$$

where P is the operator appearing in Eq. (1) and thus Eq. (3). Putting all the terms together, we obtain the global Hamiltonian

$$H = H_S + H_q + H_{qS}. \tag{7}$$

We are interested in the quantum evolution of the global system starting from the initial $t = 0$ condition

$$|\Psi_0\rangle = |q_0\rangle \otimes |0_h\rangle, \tag{8}$$

where $|q_0\rangle$ is a generic pure state of the qubit

$$|q_0\rangle = c_+|+\rangle + c_-|-\rangle, \quad |c_+|^2 + |c_-|^2 = 1, \tag{9}$$

and $|0_h\rangle$ is the ground state of the system with the Hamiltonian $H_S(h)$. The global wave function describing the quantum evolution for $t > 0$ must be a solution of the Schrödinger equation

$$i\frac{\partial}{\partial t}|\Psi(t)\rangle = H|\Psi(t)\rangle, \quad |\Psi(t=0)\rangle = |\Psi_0\rangle. \tag{10}$$

In particular, we consider a dynamic protocol arising from a sudden switching of the interaction H_{qS} between the qubit and the many-body system, at time $t = 0$, i.e., by quenching one or both of the control parameters u and v in Eq. (6) from zero to some finite value.

The above setting can be straightforwardly extended to N-level systems coupled to an environmental system S and also to the case in which the initial qubit state is mixed, and thus described by a nontrivial density matrix. Most features addressed in the rest of the paper, in particular the dynamic scaling properties, can be straightforwardly extended as well.

B. Qubit decoherence, work, and qubit-system energy exchanges

1. Coherence of the qubit

An interesting issue arising from the dynamics of the problem outlined above concerns the coherence properties of the qubit during the global quantum evolution. Starting from a pure state, the interaction with the many-body system may give rise to a loss of coherence of the qubit, depending on the properties of its density matrix

$$\rho_q(t) = {\rm Tr}_S[\rho(t)], \tag{11}$$

where $\mathrm{Tr}_S[\cdot]$ denotes the trace over the S degrees of freedom of the global (pure) quantum state

$$\rho(t) = |\Psi(t)\rangle\langle\Psi(t)|, \tag{12}$$

with $|\Psi(t)\rangle$ given by the solution of Eq. (10). Of course, $\mathrm{Tr}[\rho_q(t)] = 1$.

A good candidate to quantify the coherence properties of the qubit during its quantum evolution is provided by the so-called purity, that is, the trace of its square density matrix ρ_q,

$$\mathrm{Tr}[\rho_q(t)^2] \equiv 1 - D(t), \tag{13}$$

where we have introduced the decoherence function D such that $0 \leqslant D \leqslant 1$. This function measures the quantum decoherence, quantifying the departure from a pure state. Indeed, $D = 0$ implies that the qubit is in a pure state, and thus $D(t = 0) = 0$. The other extreme value $D = 1$ indicates that the qubit is totally unpolarized.

2. Quantum work associated with the initial quench

The initial quench, arising from turning on the interaction between the qubit q and the many-body system S, can also be characterized via the quantum work W done on the global system [14,43]. The work performed by quenching the control parameters u and v generally does not have a definite value, while it can be defined as the difference of two projective energy measurements [14]. The first one at $t = 0$ projects onto the eigenstates $|m_\mathrm{i}\rangle$ of the initial Hamiltonian H_i with a probability $p_{\mathrm{i},m}$ given by the initial density matrix. The second energy measurement projects onto the eigenstates $|n_\mathrm{f}\rangle$ of the postquench Hamiltonian H_f. Since the energy is conserved after the quench, the latter measurement can be performed at any time t during the evolution, ruled by the unitary operator $U(t, 0) = e^{-iH_\mathrm{f}t}$, without changing the distribution, in particular for $t \to 0^+$. The work probability distribution can be written as [14,44,45]

$$P(W) = \sum_{n,m} \delta[W - (E_{\mathrm{f},n} - E_{\mathrm{i},m})]|\langle n_\mathrm{f}|m_\mathrm{i}\rangle|^2 p_{\mathrm{i},m}. \tag{14}$$

The average work and its higher moments are given by

$$\langle W^k\rangle = \int dW\, W^k P(W). \tag{15}$$

As one can easily check, the average quantum work $\langle W\rangle$ can be computed by taking the difference

$$\langle W\rangle = \langle\Psi(t)|H|\Psi(t)\rangle - \langle\Psi_0|H_q + H_S|\Psi_0\rangle, \tag{16}$$

where

$$\langle\Psi_0|H_q + H_S|\Psi_0\rangle = \langle q|H_q|q\rangle + \langle 0_h|H_S|0_h\rangle \equiv E_{q0} + E_{S0}. \tag{17}$$

Since we are interested in a sudden quench at $t = 0$, we can obtain the average work from the difference of the expectation values of $H_\mathrm{f} = H$ and $H_\mathrm{i} = H_q + H_S$ on the initial state, obtaining

$$\langle W\rangle = \langle\Psi_0|H_{qS}|\Psi_0\rangle. \tag{18}$$

An analogous expression can be derived for the average of the square work, obtaining

$$\langle W^2\rangle = \langle\Psi_0|H_{qS}^2|\Psi_0\rangle. \tag{19}$$

Note that the above relatively simple equations for the first two moments of the work distribution do not extend to higher moments, i.e., $\langle W^k\rangle \neq \langle\Psi_0|H_{qS}^k|\Psi_0\rangle$ for $k > 2$. Their expressions are more complicated, requiring the computation of the whole spectrum, due to the fact that H_{qS} does not commute with the other Hamiltonian terms.

3. Energy-difference distributions

In order to study the qubit-system energy exchanges, we may consider the energy-difference distribution of the system S along the quantum evolution, associated with two energy measurements of S, at $t = 0$ and at a generic time t. We write it as

$$P_S(U, t) = \sum_{n,a,b} \delta[U - (E_{Sn} - E_{S0})]|\langle b, n|e^{-iHt}|a, 0\rangle|^2 p_a, \tag{20}$$

where $|b, n\rangle \equiv |b\rangle \otimes |n\rangle$, $|n\rangle$ and E_{Sn} indicate, respectively, eigenstates and eigenvalues of the Hamiltonian H_S (we assume a discrete spectrum, as is generally appropriate for finite-size systems), $|a\rangle$ and $|b\rangle$ indicate the eigenstates $|\pm\rangle$ of the qubit Hamiltonian, and $p_\pm = |c_\pm|^2$ are the probabilities of the initial qubit state at $t = 0$. One can check that

$$\langle U\rangle \equiv \int dy\, y\, P(y, t) = E_S(t) - E_{S0}. \tag{21}$$

More general initial distributions also may be considered, for example, associated with a bath at temperature T, replacing the initial density matrix $\rho_0 = |q, 0\rangle\langle q, 0|$ with the corresponding density matrices. Of course one may also define an analogous energy-difference distribution associated with the qubit, obtained by a two-measurement procedure on it:

$$P_q(U, t) = \sum_{n,a,b} \delta[U - (E_{qb} - E_{qa})]|\langle b, n|e^{-iHt}|a, 0\rangle|^2 p_a. \tag{22}$$

III. FINITE-SIZE SCALING FRAMEWORK

In this section we summarize the main features of the dynamic FSS framework that we will exploit to analyze the out-of-equilibrium quantum dynamics of the coupled qubit and many-body system and in particular the quantities introduced in Sec. II B. The dynamic FSS framework has been developed recently to deal with dynamic behaviors of finite-size systems at quantum transitions [35,39,46], extending equilibrium FSS frameworks to study CQTs and FOQTs [37,47–50]. This framework allows one to study the interplay among the Hamiltonian parameters, the finite linear size L, and the finite temperature T, assuming that T is sufficiently small and that the Hamiltonian parameters keep the system S close to the transition point.

A. Scaling variables at quantum transitions

The scaling hypothesis for the many-body system described by the Hamiltonian H_S is based on the existence of a nontrivial large-volume limit, keeping the appropriate scaling variables fixed. At both CQTs and FOQTs, the FSS variable related to a relevant perturbation as $H_h = hP$ [cf. Eq. (1)] can be generally written as the ratio

$$\kappa_h = E_h(L)/\Delta(L) \tag{23}$$

between the energy variation associated with the H_h term (we assume $E_h = 0$ at the transition point $h = 0$) and the energy difference of the lowest-energy states, $\Delta(L) \equiv E_1 - E_0$, at the transition point $h = 0$. Nonzero temperatures are taken into account by adding a further scaling variable

$$\tau = T/\Delta(L). \tag{24}$$

More generally, any relevant low-energy scale $\mathcal{E}$ is expected to behave as $\mathcal{E} \sim \Delta(L)$ in the FSS limit. Dynamic behaviors, exhibiting nontrivial time dependences, also require a scaling variable associated with the time variable, which is generally given by

$$\theta = \Delta(L)t. \tag{25}$$

The equilibrium and dynamic FSS limits are defined as large-size limits, keeping the above scaling variables fixed.

The outlined framework provides a unified picture of the FSS behaviors at quantum transitions, holding at both CQTs and FOQTs. Within the dynamic FSS framework, their differences are essentially related to the functional dependence of the above scaling variables on the size. Power laws generally arise at CQTs [37], while exponential laws emerge at FOQTs [47,48], in particular when boundary conditions do not favor any particular phase.

B. First-order quantum transitions

As shown by earlier works [38,47–49], the FSS behavior of isolated many-body systems at FOQTs turns out to depend greatly on the type of boundary conditions, whether they favor one of the phases or they are neutral, giving rise to FSS characterized by exponential or power-law behaviors. To simplify our presentation, in the following the system S will be taken as a quantum Ising model with boundary conditions that do not favor either of the two magnetized phases, such as periodic and open boundary conditions, which generally lead to exponential FSS laws.

The FOQT line for $g < g_c$ is related to the level crossing of the two lowest states $|\uparrow\rangle$ and $|\downarrow\rangle$ for $h = 0$ such that $\langle\uparrow|\sigma_{\boldsymbol{x}}^{(3)}|\uparrow\rangle = m_0$ and $\langle\downarrow|\sigma_{\boldsymbol{x}}^{(3)}|\downarrow\rangle = -m_0$ (independently of $\boldsymbol{x}$), with $m_0 > 0$. The degeneracy of these states is lifted by the longitudinal field h. Therefore, $h = 0$ is a FOQT point, where the longitudinal magnetization $M = L^{-d}\sum_{\boldsymbol{x}} M_{\boldsymbol{x}}$, with $M_{\boldsymbol{x}} \equiv \langle\sigma_{\boldsymbol{x}}^{(3)}\rangle$, becomes discontinuous in the infinite-volume limit. The transition separates two different phases characterized by opposite values of the magnetization m_0, i.e.,

$$\lim_{h\to 0^{\pm}} \lim_{L\to\infty} M = \pm m_0. \tag{26}$$

For one-dimensional systems [51], $m_0 = (1 - g^2)^{1/8}$.

In a finite system of size L, the two lowest states are superpositions of two magnetized states $|+\rangle$ and $|-\rangle$ such that $\langle\pm|\sigma_{\boldsymbol{x}}^{(3)}|\pm\rangle = \pm m_0$ for all sites $\boldsymbol{x}$. Due to tunneling effects, the energy gap Δ at $h = 0$ vanishes exponentially as L increases [38,52],

$$\Delta(L) \sim e^{-cL^d}, \tag{27}$$

apart from powers of L. In particular, for the one-dimensional Ising system (2) at $g < 1$, it is exponentially suppressed as [51,53]

$$\Delta(L) = 2(1 - g^2)g^L[1 + O(g^{2L})] \tag{28}$$

for open boundary conditions and

$$\Delta(L) \approx 2\sqrt{(1 - g^2)/(\pi L)}\,g^L \tag{29}$$

for periodic boundary conditions. The differences $E_i - E_0$ for the higher excited states ($i > 1$) are finite for $L \to \infty$.

Quantum Ising systems along the FOQT line develop FSS behaviors [35,39,40,46], driven by the longitudinal field h. Using Eq. (23), the corresponding scaling variable can be written as [43,47]

$$\kappa_h = \frac{2m_0 hL^d}{\Delta(L)}, \tag{30}$$

where $2m_0hL^d$ quantifies the energy associated with the corresponding longitudinal-field perturbation H_h. For example, in the equilibrium FSS limit the magnetization is expected to behave as [47] $M(h, L) = m_0\mathcal{M}(\kappa_h)$, where $\mathcal{M}$ is a FSS function.

Note that the FOQT scenario based on the avoided crossing of two levels is not realized for any boundary condition [38]: In some cases the energy difference $\Delta(L)$ of the lowest levels may even display a power-law dependence on L. However, the scaling variable κ_h obtained using the corresponding $\Delta(L)$ turns out to be appropriate as well [38].

C. Continuous quantum transitions

Finite-size scaling theories were originally developed at continuous transitions (see, e.g., Refs. [37,54,55] and references therein). The CQT of the Ising model [cf. Eqs. (2) and (3)] is characterized by two relevant parameters, $r \equiv g - g_c$ and h (such that they vanish at the critical point), with renormalization-group dimensions y_r and y_h, respectively. The relevant FSS variables are

$$\kappa_r = L^{y_r} r, \quad \kappa_h = L^{y_h} h. \tag{31}$$

The FSS limit is obtained by taking $L \to \infty$ and keeping κ_r and κ_h fixed.

Note that the expression for κ_h in Eq. (31) can be obtained using the more general definition (23). Indeed, at CQTs the energy variation arising from the perturbation $H_h = h\sum_{\boldsymbol{x}} P_{\boldsymbol{x}}$, with $P_{\boldsymbol{x}} = -\sigma_{\boldsymbol{x}}^{(3)}$, is given by

$$E_h(L) \sim hL^{d-y_p}, \tag{32}$$

where y_p is the renormalization-group critical dimension of the local operators $P_{\boldsymbol{x}}$ at the fixed point describing the quantum critical behavior. Moreover, we have

$$\Delta(L) \sim L^{-z}, \tag{33}$$

where z is the universal dynamic exponent. Then, using the scaling relation among critical exponents [24,37]

$$y_h + y_p = d + z, \tag{34}$$

where y_h is the renormalization-group dimension of the perturbation h, we end up with the expression of κ_h reported in Eq. (31). An analogous derivation can be obtained for κ_r.

The equilibrium critical exponents y_r and y_h of the quantum Ising model are those of the $(d+1)$-dimensional Ising universality class [24,41,42]. Therefore, for one-dimensional systems they are $y_r = 1/\nu = 1$ and $y_h = (d + z + 2 - \eta)/2 = (4 - \eta)/2$ with $\eta = 1/4$. For two-dimensional models the critical exponents are not known exactly, but there are very accurate estimates (see, e.g., Refs. [56–60]); in particular [59] $y_r = 1/\nu$ with $\nu = 0.629\,971(4)$ and $y_h = (5 - \eta)/2$ with $\eta = 0.036\,298(2)$. For three-dimensional systems they assume mean-field values $y_r = 2$ and $y_h = 3$ apart from logarithms. The temperature T gives rise to a relevant perturbation at CQTs associated with the scaling variable $\tau = L^z T$, where $z = 1$ (for any spatial dimension) is the dynamic exponent characterizing the behavior of the energy differences of the lowest-energy states and in particular the gap $\Delta \sim L^{-z}$.

A generic observable O in the FSS limit behaves as

$$O(r, h, L) \approx L^{-y_o} \mathcal{O}(\kappa_r, \kappa_h), \tag{35}$$

where the exponent y_o is the renormalization-group dimension associated with O and $\mathcal{O}$ is a universal equilibrium FSS function. The approach to such an asymptotic behavior is characterized by power-law corrections, typically controlled by irrelevant perturbations at the corresponding fixed point [37]. The equilibrium FSS at quantum transitions has been extended also to quantum-information concepts [61–65], such as the ground-state fidelity and its susceptibility, which measure the change of the ground state when varying the Hamiltonian parameters around a quantum transition [50].

D. Disordered phase

One may compare the above scaling behaviors with those expected when the system S is not close to a phase transition, for example, for $g > g_c$ in the case of quantum Ising models. In this region the system is in the disordered phase, where the length scale ξ of the correlations is finite. In particular, close to the transition point g_c, it behaves as $\xi \sim (g - g_c)^{-\nu}$. Thus the ratio L/ξ diverges in the large-L limit. The many-body system appears as effectively composed of $(L/\xi)^d$ uncorrelated subsystems. The gap $\Delta(L)$ remains finite with increasing L. Close to the CQT, i.e., for $g \gtrsim g_c$, it behaves as $\Delta \sim \xi^{-z}$.

IV. DYNAMIC FSS *ANSATZ* FOR THE QUBIT-SYSTEM SETUP

The dynamic processes arising from the instantaneous turning on of the interaction term H_{qS} can be described within a dynamic FSS framework, extending the framework outlined in Sec. III, to take into account the interaction of the many-body system S with the qubit q. Besides the scaling variable κ_h [cf. Eq. (23)] we also need to consider scaling variables associated with the other parameters of the global Hamiltonian H, i.e., u, v, and δ.

Since both u and v terms are coupled to the operator P contained in the h term of the global Hamiltonian (1), we expect the corresponding scaling variables to scale analogously as κ_h. They can thus be obtained by replacing h with u (or v) in the definition of κ_h. Given that κ_h is linear in h, one has

$$\kappa_u = u\kappa_h/h, \quad \kappa_v = v\kappa_h/h. \tag{36}$$

We must also associate a FSS variable with the energy difference δ of the eigenstates of the qubit Hamiltonian H_q,

$$\varepsilon_\delta = \delta/\Delta(L), \tag{37}$$

since δ is a further energy scale of the problem. Finally, the scaling variable $\theta = \Delta(L)t$ is associated with the time variable.

A. Qubit decoherence functions

Let us first address the issue of the decoherence properties of the qubit along the global quantum evolution arising from the interaction with the system S. The dynamic scaling behavior of the decoherence function $D(t)$ [cf. Eq. (13)], as a function of time, size, and Hamiltonian parameters of the system S, has been discussed in Ref. [35] in the simplest case where $\delta = 0$ (i.e., the qubit Hamiltonian is trivial). As detailed in Appendix A, each time $[H_q, H_{qS}] = 0$ [as is the case for $v = 0$ in Eq. (6)], $D(t)$ does not depend on the qubit spectrum. We thus expect the same dynamic FSS behavior reported in Ref. [35],

$$D(u, h, L, t) = \mathcal{D}(\kappa_u, \kappa_h, \theta), \tag{38}$$

which is independent of δ, and therefore of ε_δ. For small values of the coupling u, we have that

$$D(u, h, L, t) = \tfrac{1}{2} u^2 Q(h, L, t) + O(u^3), \tag{39}$$

where the growth-rate function Q measures the sensitivity of the qubit coherence properties to the coupling u. Its scaling behavior can be derived by matching that of $\mathcal{D}$ in Eq. (38), obtaining [35]

$$Q(h, L, t) \approx \left(\frac{\partial \kappa_u}{\partial u}\right)^2 \mathcal{Q}(\kappa_h, \theta). \tag{40}$$

We now focus on the more general case $[H_q, H_{qS}] \neq 0$, restricted to the case $u = 0$ for simplicity, without loss of generality. The most natural working hypothesis is that analogous scaling behaviors develop, with a further dependence on the scaling variable ε_δ in Eq. (37) and replacing κ_u with κ_v. One is then led to put forward the following FSS behavior:

$$D(\delta, v, h, L, t) = \mathcal{D}(\varepsilon_\delta, \kappa_v, \kappa_h, \theta). \tag{41}$$

Assuming again analyticity at $v = 0$ and since $D \geqslant 0$, one expects an expansion analogous to Eq. (39),

$$D(\delta, v, h, L, t) = \tfrac{1}{2} v^2 Q(\delta, h, L, t) + O(v^3), \tag{42}$$

which can be matched to the scaling behavior in Eq. (41) to obtain

$$Q(\delta, h, L, t) \approx \left(\frac{\partial \kappa_v}{\partial v}\right)^2 \mathcal{Q}(\varepsilon_\delta, \kappa_h, \theta). \tag{43}$$

Notice that the scaling relations for the growth-rate function Q imply a power law for CQTs, i.e.,

$$Q(h, L, t) \approx L^{2y_h} \mathcal{Q}(\varepsilon_\delta, \kappa_h, \theta), \tag{44}$$

while exponential laws arise at FOQTs (when considering neutral boundary conditions), such as

$$Q(h, L, t) \approx \frac{L^{2d}}{\Delta(L)^2} \mathcal{Q}(\varepsilon_\delta, \kappa_h, \theta), \tag{45}$$

thus increasing as $\sim \exp(bL^d)$.

One may compare the above scaling behaviors with those expected when the system S is not close to a phase transition, for example, for $g > g_c$ in the case of the quantum Ising models. Taking into account that Q is equivalent to a generalized susceptibility, the arguments reported in Sec. III D lead us to the expectation that the growth-rate function should increase as the volume of the system S, i.e.,

$$Q \sim L^d. \tag{46}$$

The above scaling relations (44) and (45) demonstrate that the rate of the qubit decoherence gets enhanced when the system S experiences a quantum transition. For example, we may compare the L^d behavior expected in the disordered phase with the significantly faster increase L^{2y_h} at $g = g_c$ where the system is critical [cf. Eq. (44)] due to the fact that ($z = 1$)

$$2y_h = d + z + 2 - \eta = d + 3 - \eta > d. \tag{47}$$

We finally note that the scaling behavior in the critical region $g - g_c \ll 1$, where $\xi \approx (g - g_c)^{-\nu} \gg 1$, can be inferred by standard scaling arguments. It essentially amounts to replacing L with ξ in the dynamic FSS equations.

B. Quantum work associated with the initial quench

We now discuss the scaling behavior of the quantum work associated with the initial quench of the interaction term H_{qS}. We explicitly address the first and the second moment of the work probability distribution defined in Eq. (14), but similar arguments can be put forward for the higher moments, as defined in Eq. (15).

To begin with, we report the scaling *Ansätze* of the average work and average square work which are expected in the simplest case $[H_q, H_{qS}] = 0$ (for $v = 0$):

$$\langle W \rangle(\delta, u, h, L) \approx \Delta(L) \mathcal{W}_1(\kappa_u, \kappa_h), \tag{48a}$$

$$\langle W^2 \rangle(\delta, u, h, L) \approx \Delta(L)^2 \mathcal{W}_2(\kappa_u, \kappa_h). \tag{48b}$$

These are independent of the spectrum of the qubit, and in particular of δ (analogous expressions hold for higher powers of the work). In the case of CQTs, this *Ansatz* is supported by equilibrium FSS arguments, exploiting Eq. (A11). Indeed, since

$$\langle 0_h | P | 0_h \rangle \approx L^{d - y_p} f_P(\kappa_h), \tag{49}$$

it is easy to see that simple calculations lead to Eq. (48a) with $\mathcal{W}_1(\kappa_u, \kappa_h) \propto \kappa_u f_P(\kappa_h)$.

In the more general case $[H_q, H_{qS}] \neq 0$, we expect that the scaling variable ε_δ associated with the gap δ of the qubit Hamiltonian should also affect the dynamic FSS behavior. However, for the average and the average square work [cf. Eqs. (18) and (19), respectively], this is not the case:

$$\langle W \rangle(\delta, u, v, h, L) \approx \Delta(L) \mathcal{W}_1(\kappa_u, \kappa_v, \kappa_h), \tag{50a}$$

$$\langle W^2 \rangle(\delta, u, v, h, L) \approx \Delta(L)^2 \mathcal{W}_2(\kappa_u, \kappa_v, \kappa_h). \tag{50b}$$

Higher moments are expected to generally depend on ε_δ too.

C. Time dependence of the energy exchanges

Returning to the energy distribution defined in Eq. (20), let us again begin with the simplest case $v = 0$. We expect the scaling behavior

$$P_S(U, u, h, L, t) \approx \Delta(L)^{-1} \mathcal{P}(\upsilon, \kappa_u, \kappa_h, \theta), \tag{51}$$

where

$$\upsilon = U/\Delta(L). \tag{52}$$

Thus the average of U and its fluctuations $\langle U^2 \rangle_c = \langle U^2 \rangle - \langle U \rangle^2$ should scale, respectively, as

$$\langle U \rangle(u, h, L, t) \approx \Delta(L)\, \mathcal{U}_1(\kappa_u, \kappa_h, \theta), \tag{53a}$$

$$\langle U^2 \rangle_c(u, h, L, t) \approx \Delta(L)^2\, \mathcal{U}_2(\kappa_u, \kappa_h, \theta). \tag{53b}$$

In the most general case $v \neq 0$, one should add a further dependence on the scaling variable ε_δ associated with the gap of the qubit Hamiltonian. Therefore, we obtain

$$P_S(U, \delta, u, v, h, L, t) \approx \Delta(L)^{-1} \mathcal{P}(\upsilon, \varepsilon_\delta, \kappa_u, \kappa_v, \kappa_h, \theta). \tag{54}$$

V. DYNAMIC BEHAVIOR AT THE CQT

We have seen that the dynamic FSS theory specialized to the qubit-system setup predicts a nontrivial scaling limit for the different properties of the model. Here we focus on the behavior at the CQT of the one-dimensional Ising model and present the results of numerical exact diagonalization simulations for the dynamics of a qubit, after it is suddenly and homogeneously coupled to an Ising ring with Hamiltonian (2). We recall that, as detailed in Appendix A, for $v = 0$ the qubit exhibits pure dephasing in time while the system evolves in two independent branches with the same Hamiltonian form and different fields [27,28] [cf. Eq. (A2)]. A dynamic FSS theory for the decoherence functions of the qubit coupled to a many-body system at a quantum transition has been already addressed in the literature, in this specific case and for $\delta = 0$ [35].

Here let us discuss the general case in which the Hamiltonian coupling term H_{qS} does not commute with the qubit Hamiltonian H_q, i.e., $u = 0$ and $v \neq 0$ in Eq. (6). In passing we note that the complexity of the numerical approaches discussed below is not affected by an eventual nonzero value of u, since they require the manipulation of the full Hilbert space of the system. We simulated setups where the Ising ring consists of up to $L = 24$ sites for static calculations, while we limited ourselves to $L = 16$ sites for the dynamics of such systems. As we will see below, the dynamic FSS scaling behavior turns out to emerge quite neatly already for these moderate lengths, thus making unnecessary, in practice, any further extensive check at larger size. A full exact diagonalization approach has

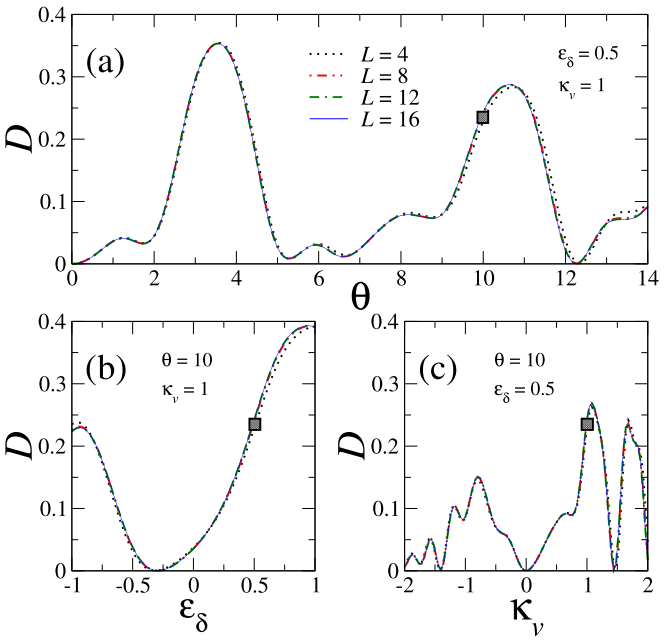

FIG. 1. Decoherence function D for a qubit coupled to Ising spin-chain systems of different lengths L (see the legend) at the CQT ($g = g_c = 1$). All numerical data presented here and in the following figures are for a qubit-system coupling realized through $u = 0$ and $v \neq 0$ in Eq. (6) such that $[H_q, H_{qS}] \neq 0$. The three panels display the behavior of D as a function of various scaling variables, according to the following scheme: (a) $\varepsilon_\delta = 0.5$, $\kappa_v = 1$, and varying θ; (b) $\kappa_v = 1$, $\theta = 10$, and varying ε_δ; and (c) $\varepsilon_\delta = 0.5$, $\theta = 10$, and varying κ_v. In all simulations we fixed $\kappa_h = 0.8$ and $u = 0$, while the qubit was initialized with $c_+ = \sqrt{2/3}$. To facilitate the readability, we kept the same scaling variables in all the panels, specified in the legend, except the one entering the x axis. The dark square in each panel corresponds to a common point in all plots.

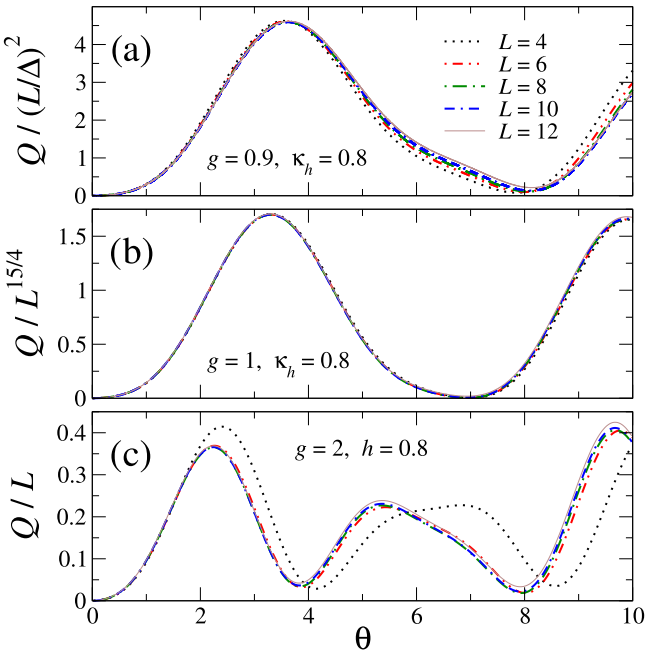

FIG. 2. Scaling of the growth-rate function Q as a function of time, for three distinct situations: (a) on the FOQT line, for $g = 0.9$; (b) at the CQT, for $g = g_c = 1$; and (c) in the disordered phase, for $g = 2$. The evaluated growth-rate function quantifies the sensitivity of the qubit coherence to the coupling v. We also fixed $\varepsilon_\delta = 0.5$ and set the initial state as $c_+ = \sqrt{2/3}$. The longitudinal field h has been chosen without loss of generality in such a way that (a) and (b) $\kappa_h = 0.8$ and (c) $h = 0.8$.

been used for systems with $L \leqslant 12$, while a Lanczos diagonalization followed by a fourth-order Runge-Kutta integration of the unitary-evolution operator was employed for larger sizes ($13 \leqslant L \leqslant 16$). We carefully checked that, for most of the simulations, a time step $dt = 10^{-3}$ is sufficient to reach a high degree of convergence. As we will explain below, for the calculation of second-order temporal fluctuations of the statistics of energy exchanges, at the largest size considered, a smaller time step $dt = 10^{-4}$ turns out to be required.

We start with the analysis of the qubit decoherence function D defined in Eq. (11). Figure 1 displays the scaling behavior of D as a function of several different scaling variables, namely, the rescaled time θ [Fig. 1(a)], the qubit detuning ε_δ [Fig. 1(b)], and the qubit-system coupling κ_v [Fig. 1(c)]. Remarkably, data collapse appears already for Ising-chain systems of $L \lesssim 10$ sites, as is evident from the figure. This validates the *Ansatz* put forward in Eq. (41). We note that the strongly oscillating behavior which emerges as a function of θ, implying nearly perfect revivals of the coherence at short times (e.g., at $\theta \approx 5.3, 6.6, 12.3$ in the figure), is due to the fact that the dynamic FSS framework is probing the postquench dynamics of a qubit coupled to a many-body system within the critical regime of a quantum transition. In particular, for a fixed value of the rescaled qubit-system coupling (e.g., $\kappa_v = 1$ in the figure) the corresponding coupling parameter v entering H_{qS} scales to zero polynomially with L [recall Eqs. (36) and (23)]. Therefore, as observed in Refs. [35,39], one expects the global system not to thermalize, and thus a complete decoherence of the qubit not to occur, for finite and fixed rescaled coupling constants.

A similar reasoning can be drawn for the decoherence growth-rate function Q, which is defined as the second derivative of D with respect to the qubit-system coupling parameter u or v [cf. Eqs. (39) and (42), respectively]. Specifically, we have numerically computed the second derivative of D with respect to v, through the evaluation of finite differences obtained by varying κ_v around zero of a small step $\delta\kappa_v = \pm 10^{-3}$ (results are stable to the choice of $\delta\kappa_v$ around such a value). The numerical outcomes of Fig. 2 display the temporal behavior of Q in three different situations, namely, at a FOQT [Fig. 2(a); cf. Eq. (45)], at the CQT point [Fig. 2(b); cf. Eq. (44)], and in the disordered phase [Fig. 2(c); cf. Eq. (46)]. A direct comparison of the various scaling behaviors, which again present a notable data collapse at small sizes, reveals a dependence on the chain length L, which turns from exponential (at the FOQT, $g < 1$) to power law proportional to $L^{15/4}$ (at the CQT, $g = g_c = 1$) or proportional to L (in the disordered phase, $g > 1$).

Other properties that we analyzed are related to the statistics associated with the energy injected by quenching the interaction strength H_{qS} and with the energy distribution of

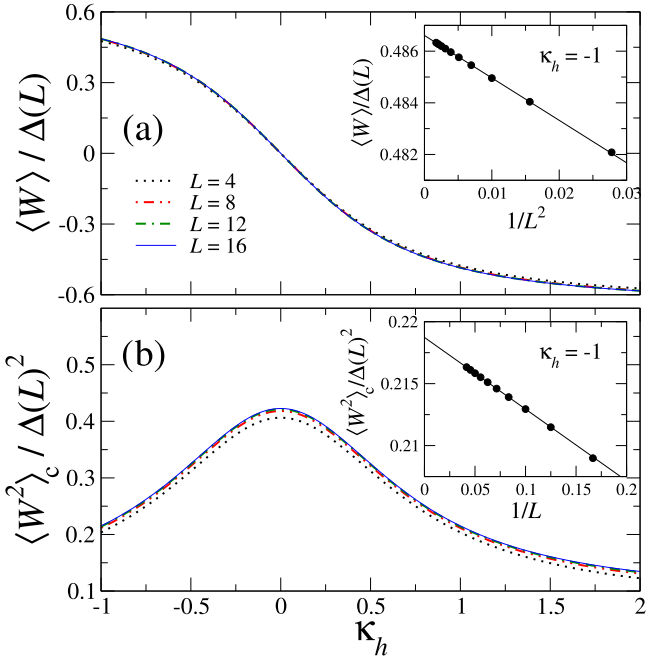

FIG. 3. Scaling behavior of (a) the average work $\langle W \rangle$ and (b) the variance of the work distribution $\langle W^2 \rangle_c = \langle W^2 \rangle - \langle W \rangle^2$, done by quenching the qubit-system interaction from zero to $\kappa_v = 1$, as a function of the rescaled longitudinal field κ_h. The system (Ising chain) is at the CQT point $g = g_c = 1$ and $\varepsilon_\delta = 0.5$, while $c_+ = \sqrt{2/3}$. The two insets show the convergence with the system size up to $L = 24$, at fixed $\kappa_h = -1$, of the average and of the variance of the work, respectively, showing dominant contributions in L^{-2} and L^{-1} (solid lines are fits of numerical data).

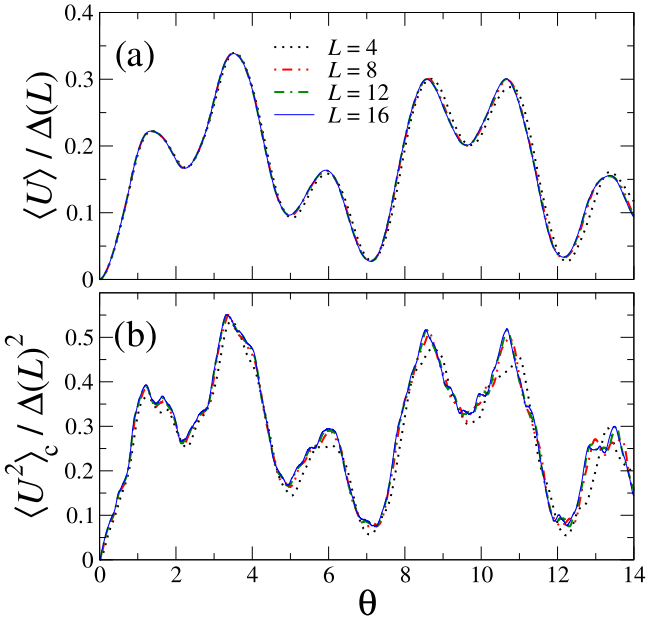

FIG. 4. Scaling behavior in time of the energy-difference distribution of an Ising-chain system S at the CQT, coupled to a qubit: (a) the average energy difference $\langle U \rangle$ and (b) its fluctuations $\langle U^2 \rangle_c = \langle U^2 \rangle - \langle U \rangle^2$. The other scaling variables and the initial state have been set as in Fig. 1(a).

the system S during the time evolution. In Fig. 3 we show the average work $\langle W \rangle$ [Fig. 3(a)] and the variance of the work distribution $\langle W^2 \rangle_c = \langle W^2 \rangle - \langle W \rangle^2$ [Fig. 3(b)] done by the quench in the qubit-system setup, as a function of the rescaled longitudinal field κ_h in the Ising-chain system at its CQT, for fixed ϵ_δ. In analogy to the decoherence properties of the qubit, numerical results indicate a nice scaling behavior, thus confirming the dynamic FSS *Ansätze* of Eqs. (50). A closer look at finite-size corrections for fixed κ_h reveals an approach to the asymptotic behavior which is characterized by $O(L^{-2})$ and $O(L^{-1})$ corrections, respectively (see the two insets). This reflects a slower approach to the expected asymptotic behavior of $\langle W^2 \rangle_c$, rather than that of $\langle W \rangle$, as is qualitatively visible by comparing the two main figures. These data suggest that the global convergence of full work statistics to its dynamic FSS may be $O(L^{-1})$, as already pointed out in Ref. [46].

In an analogous spirit, it would be interesting to analyze the first two moments of the energy-difference distribution of the Ising system S along the dynamics at the CQT [cf. Eq. (20)]. Specifically, the behavior with respect to the rescaled time θ of the average energy difference $\langle U \rangle$ and of its fluctuations $\langle U^2 \rangle_c = \langle U^2 \rangle - \langle U \rangle^2$ is shown in Figs. 4(a) and 4(b), respectively. We observe nice convergence to the dynamic FSS behavior predicted by Eqs. (53). We also observe that the calculation of fluctuations is very sensitive to the numerical accuracy of the simulated dynamics, essentially because much larger precision is required when computing connected quantities, generally arising from large cancellations of their terms.

We point out that the numerical results presented in this section have been obtained by fixing the same initial state and adopting specific values for the various scaling variables (for details, see the insets of the various figures). However, we have also performed simulations using other sets of parameters (not shown) and carefully checked that all our conclusions are not affected by such choices.

VI. DYNAMIC BEHAVIOR AT THE FOQT

A. Two-level reduction of the system S

We now turn to a situation where the Ising-chain system S is along the FOQT line ($g < g_c$) and concentrate on boundary conditions which do not favor any particular phase. In such a case, one can try to simplify the description of the global system by employing a two-level approximation for the system S, as was done in Refs. [39,40], in different contexts. Under the assumption that only the lowest levels of the system S are effectively involved in the dynamic behavior arising from the sudden quench of the qubit-system interaction in the dynamic FSS limit, we may consider the two-level reduction of the Hamiltonian H_S,

$$H_{S_2}(h) = -\frac{\beta}{2}\sigma^{(3)} + \frac{\gamma}{2}\sigma^{(1)},$$
$$\beta = 2m_0 h L^d, \ \gamma = \Delta(L), \ \kappa_h = \beta/\gamma, \qquad (55)$$

which acts on two-component wave functions, corresponding to the states $|+\rangle$ and $|-\rangle$ such that $\sigma^{(3)}|\pm\rangle = \pm|\pm\rangle$. Then the

qubit-system interaction term becomes

$$H_{qS_2} = -\frac{\zeta}{2}\Sigma^{(1)}\sigma^{(3)} - \frac{\eta}{2}\Sigma^{(3)}\sigma^{(3)},$$
$$\eta = 2m_0 L^d u,\ \kappa_u = \eta/\gamma,$$
$$\zeta = 2m_0 L^d v,\ \kappa_v = \zeta/\gamma. \tag{56}$$

The above Hamiltonian terms are completed by the qubit Hamiltonian, which we can be written as

$$H_q = \tfrac{1}{2}\delta\Sigma^{(3)}, \quad \varepsilon_\delta = \delta/\gamma, \tag{57}$$

neglecting the irrelevant identity term of Eq. (6). Therefore, in this approximation, the global Hamiltonian is given by

$$H_2 = H_{S_2} + H_q + H_{qS_2}, \tag{58}$$

to be compared with Eq. (7).

Within the two-level approximation for the system S at a FOQT, we may thus write the global Hamiltonian as

$$\hat{H}_2 \equiv \frac{H_2}{\gamma} = -\frac{\kappa_h}{2}\sigma^{(3)} + \frac{1}{2}\sigma^{(1)} + \frac{\varepsilon_\delta}{2}\Sigma^{(3)} - \frac{\kappa_u}{2}\Sigma^{(3)}\sigma^{(3)} - \frac{\kappa_v}{2}\Sigma^{(1)}\sigma^{(3)}, \tag{59}$$

or, using the bases where both $\Sigma^{(3)}$ and $\sigma^{(3)}$ are diagonal over the qubit and S states, we may write $\hat{H}_2$ as the 4×4 matrix

$$\frac{1}{2}\begin{pmatrix} \varepsilon_\delta - \kappa_{h+u} & 1 & -\kappa_v & 0 \\ 1 & \varepsilon_\delta + \kappa_{h+u} & 0 & \kappa_v \\ -\kappa_v & 0 & -\varepsilon_\delta - \kappa_{h-u} & 1 \\ 0 & \kappa_v & 1 & -\varepsilon_\delta + \kappa_{h-u} \end{pmatrix}, \tag{60}$$

with $\kappa_{h\pm u} \equiv \kappa_h \pm \kappa_u$. Note that the Hamiltonian (59) allows us to write the corresponding Schrödinger problem in terms of scaling variables only, i.e.,

$$i\frac{\partial}{\partial\theta}|\psi(\theta)\rangle = \hat{H}_2|\psi(\theta)\rangle, \quad \theta = \gamma t, \tag{61}$$

where $|\psi(\theta)\rangle$ denotes the wave function of the global system in the reduced four-dimensional Hilbert space. Equation (61) readily implies that, under the two-level reduction approximation for the system S, the dynamic FSS behavior put forward in Sec. IV is automatically guaranteed.

B. Numerical results

We now report a numerical verification of the dynamic FSS behavior outlined in Sec. IV within the one-dimensional Ising model along its FOQT line and the comparison with the results of the two-level approximation of the system S.

We start by commenting on the simpler case $u \neq 0$ and $v = 0$, where the qubit Hamiltonian commutes with the interaction term. In such a case, one can compute the corresponding FSS functions in an analytic form. Indeed, the matrix representation (60) of $\hat{H}_2$ reduces to a 2×2 block diagonal form, for which analytic expressions can be obtained. Appendix A 2 reports the dynamic FSS functions of all the quantities defined in Sec. II B.

The analytic calculations for the less trivial case, $u = 0$ and $v \neq 0$, for which $[H_q, H_{qS_2}] \neq 0$, are more cumbersome.

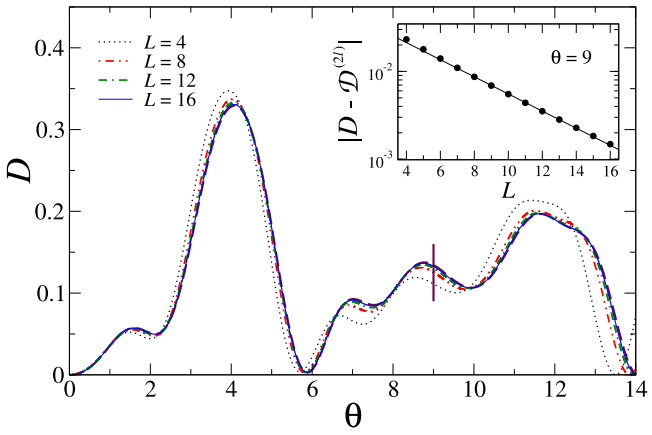

FIG. 5. Decoherence function D for a qubit coupled to an Ising spin chain at the FOQT ($g = 0.9$), as a function of the rescaled time θ. We fixed $\kappa_v = 1$ and $\varepsilon_\delta = 0.5$ and set the initial state with $c_+ = \sqrt{2/3}$, as in Fig. 1(a). The inset shows numerical data for $\theta = 9$, supporting an exponential convergence to the prediction $\mathcal{D}^{(2l)}$ given by the two-level approximation for the Ising chain (thick dashed line in the main panel).

Indeed, the solution of the corresponding quantum problem requires the diagonalization of the full 4×4 matrix Hamiltonian (60) over the four-dimensional Hilbert space of the qubit and two levels associated with S. The analytical results are not very illuminating, and for this reason we decided not to report them here. In contrast, we prefer to concentrate on a quantitative comparison between the outcomes of numerical exact diagonalization simulations for the full many-body Hamiltonian H and those of the reduced 4×4 setup $\hat{H}_2$.

The analysis of the dynamic FSS for the decoherence function D as a function of the rescaled time θ, when coupled to the Ising spin chain at the FOQT, is reported in Fig. 5, where we plotted the outcomes of the simulation of the full model. They demonstrate a clear qualitative accordance with those of the two-level approximation $\mathcal{D}^{(2l)}(\theta)$, obtained by solving Eq. (61) (brown long-dashed line). We notice the appearance of strong revivals, as is the case in proximity to a CQT (cf. Fig. 1). The convergence in L to the analytic two-level approximation appears to be exponential, as shown by the inset in Fig. 5 for a fixed value of $\theta = 9$.

We now look at the statistics of energy exchanges. The first two moments of the statistics of the work, for the Ising-chain system at the FOQT, are reported in Fig. 6. Data collapse to a dynamic FSS behavior in the infinite volume is clearly evident. However, while the average work $\langle W\rangle$ nicely converges to the two-level prediction $\mathcal{W}^{(2l)}$, with an apparent exponential dependence on L [Fig. 6(a) and its inset], this is not the case for the work fluctuations $\langle W^2\rangle_c$ [Fig. 6(b)]. Specifically, the two-level prediction $\mathcal{W}^{(2l)}_{2c}$ is apparently off from the expected limiting behavior. In fact, the inset hints at an $O(L^{-1})$ convergence of the discrepancy to a value which is different from zero, thus implying the failure of the two-level reduction of the system S in exactly grasping the asymptotic behavior of the higher momenta of the work statistics. Further details on the accuracy of the two-level approximation are given in Appendix B.

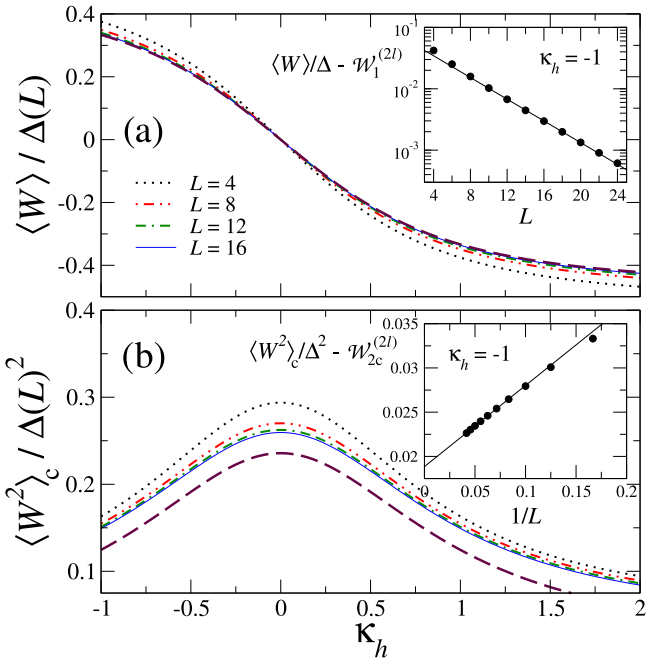

FIG. 6. Same as in Fig. 3, but for a qubit coupled to an Ising spin-chain system S at the FOQT, with $g = 0.9$. Curves are shown for (a) the average work and (b) its fluctuations. Thick dashed lines denote the predictions (a) $\mathcal{W}_1^{(2l)}$ and (b) $\mathcal{W}_{2c}^{(2l)}$, given by replacing S with an approximate two-level model. The inset in (a) displays an exponential convergence in L of the ratio $\langle W \rangle / \Delta(L)$ to the two-level prediction $\mathcal{W}_1^{(2l)}$. The inset in (b) shows the behavior in L of the difference between the work fluctuations $\langle W^2 \rangle_c / \Delta(L)^2$ and the two-level prediction $\mathcal{W}_{2c}^{(2l)}$. In this case, an L^{-1} fit of the numerical data leads to a finite discrepancy of $1.89(1) \times 10^{-2}$ in the infinite-volume limit. In both insets we fixed $\kappa_h = -1$.

Finally, in Fig. 7 we repeat the analysis of the statistics of the energy-difference distribution in the system S, where similar conclusions apply. In particular, we display the temporal behavior of the average [Fig. 7(a)] and of its fluctuations [Fig. 7(b)]. Analogously to the outcomes we found at the CQT (cf. Fig. 4), we observe that fluctuations $\langle U^2 \rangle_c$ are very sensitive to the accuracy of the simulation. It is also worth noticing that the long-dashed curves which indicate the two-level predictions ($\mathcal{U}_1^{(2l)}$ and $\mathcal{U}_2^{(2l)}$, respectively) follow the same behavior with θ. More precisely, it can be shown that the ratio

$$\mathcal{U}_2^{(2l)} / \mathcal{U}_1^{(2l)} = \sqrt{1 + \kappa_h^2} \tag{62}$$

depends only on the value of κ_h (in the figure we used $\kappa_h = 0.8$; therefore $\sqrt{1 + \kappa_h^2} \approx 1.28$). This is in analogy to Eq. (A25), which can be easily proven for a longitudinal qubit-system interaction ($v = 0$).

Before ending we stress that, similarly to the dynamic behavior at the CQT, analogous results have been obtained (in particular the collapse of numerical data to the FSS behavior put forward in Sec. III B) for other values of scaling variables and initial states.

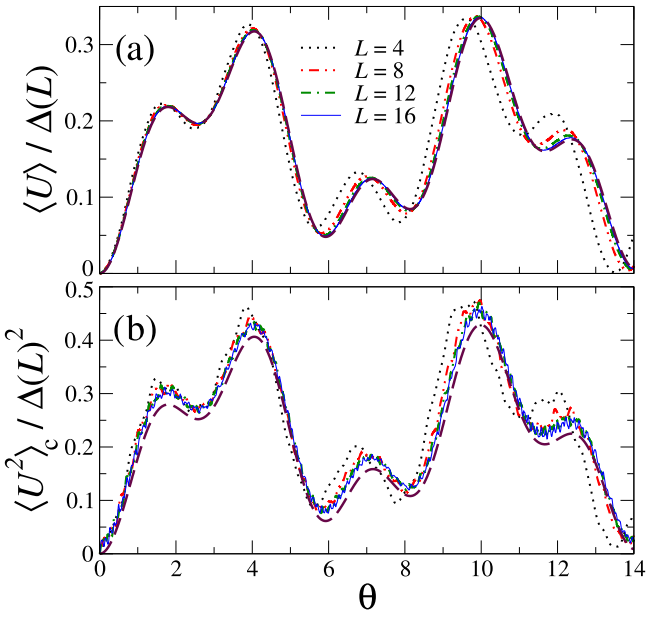

FIG. 7. Same as in Fig. 4, but for a qubit coupled to an Ising-chain system at the FOQT, with $g = 0.9$. Thick dashed lines denote the predictions (a) $\mathcal{U}_1^{(2l)}$ and (b) $\mathcal{U}_2^{(2l)}$, given by replacing S with an approximate two-level model as depicted in Sec. VI A. A small Runge-Kutta time step of $dt = 10^{-4}$ was employed in order to guarantee the numerical accuracy of the results plotted in (b).

VII. CONCLUSION

We have addressed the quantum dynamics of a system composed of a qubit globally coupled to a many-body system characterized by short-range interactions. We employed a dynamic FSS framework to investigate the out-of-equilibrium dynamics arising from the sudden variation (turning on) of the interaction between the qubit and the many-body system, in particular when the latter is in proximity to a quantum first-order or a continuous phase transition. Although the approach is quite general, we considered d-dimensional quantum Ising spin models in the presence of transverse and longitudinal fields, as paradigmatic quantum many-body systems.

To characterize the out-of-equilibrium dynamics, we focused on a number of quantum-information-oriented properties of the model. Generalizing the results of Ref. [35], we considered the information and energy flow among the various parts of the composite system: We studied the decoherence of the qubit and the statistics associated with the energy injected by switching on the qubit-system interaction and with the energy distribution of the system during the temporal evolution. When the many-body system S was close to a quantum transition, either at a CQT or at a FOQT, we derived the asymptotic scaling behavior exploiting the dynamic FSS framework. The scaling behaviors of the above quantities were validated by means of extensive numerical simulations specialized to one-dimensional Ising systems. We always observed convergence to the expected asymptotic FSS behavior when the system S was at both CQTs and FOQTs.

In the case of FOQTs, we also employed a two-level approximation for the many-body system S to compute the dynamic FSS functions associated with the out-of-equilibrium

quantum evolution. The agreement with the numerical results was satisfactory. Quantitative differences between the numerics and the two-level approximation emerged only when monitoring fluctuations and higher momenta of the various energy statistics.

It is however worth pointing out that, already with ten spins, it is possible to infer the asymptotic FSS behavior with fair accuracy. This paves the way toward an experimental probe of the influence of criticality on the quantum transport properties, spurred on by the recent developments in quantum technologies with ultracold atoms and ions. Indeed, they already demonstrated the capability to faithfully reproduce the unitary dynamics of quantum Ising-like chains with approximately ten spins [66–72].

Finally, we mention that it is possible to extend our dynamic FSS analysis to more general situations. Besides those based on sudden variations of the interactions between the qubit and the many-body system, one may consider other dynamic protocols, for example, by taking the opposite limit of slow changes. This situation can be also analyzed within appropriate FSS frameworks, such as that considered in Ref. [40]. We may also devise extensions to more general models, where the qubit is replaced by a generic N-level quantum system, the environment is mapped in the continuum limit (or, more generally, can be modeled by a many-body system presenting CQTs or FOQTs), and the qubit-system coupling is not homogeneous or may have a different and more complicated shape.

APPENDIX A: THE COMMUTATIVE CASE $[H_q, H_{qS}] = 0$

1. General features

A particular case of the general problem outlined in Sec. II is realized when $v = 0$ in the qubit-system Hamiltonian (6), i.e.,

$$H_{qS} = u\Sigma^{(3)}P, \tag{A1}$$

which implies $[H_q, H_{qS}] = 0$. This condition allows us to write the time evolution of the global system in terms of dynamic evolutions of the system S only. Indeed, one can easily prove that the solution of the corresponding Schrödinger problem is given by

$$\begin{aligned}|\Psi(t)\rangle = {} & e^{-i\epsilon_+ t}c_+|+\rangle \otimes |\Phi_{h+u}(t)\rangle \\ & + e^{-i\epsilon_- t}c_-|-\rangle \otimes |\Phi_{h-u}(t)\rangle,\end{aligned} \tag{A2}$$

where

$$|\Phi_{h\pm u}(t)\rangle = e^{-iH_S(h\pm u)t}|0_h\rangle, \tag{A3}$$

i.e., they are solutions of the Schrödinger equations for the system S only,

$$i\frac{\partial}{\partial t}|\Phi_{h\pm u}(t)\rangle = H_S(h \pm u)|\Phi_{h\pm u}(t)\rangle, \tag{A4}$$

with $|\Phi_{h\pm u}(t = 0)\rangle = |0_h\rangle$.

Notable relations can be obtained by focusing on the evolution of the qubit only. The elements of its reduced density matrix [cf. Eq. (11)] read

$$\begin{aligned}&\rho_{q,11}(t) = |c_+|^2, \quad \rho_{q,22}(t) = |c_-|^2, \\ &\rho_{q,12}(t) = e^{-i\delta t}c_-^* c_+ \langle \Phi_{h-u}(t)|\Phi_{h+u}(t)\rangle = \rho_{q,21}(t)^*.\end{aligned} \tag{A5}$$

The decoherence function $D(t)$ [cf. Eq. (13)] can be written as

$$D(t) = 2|c_+|^2|c_-|^2 F_D(t), \tag{A6}$$

where

$$F_D(t) = 1 - |\langle \Phi_{h-u}(t)|\Phi_{h+u}(t)\rangle|^2 \tag{A7}$$

and $0 \leqslant F_D(t) \leqslant 1$. The function F_D measures the quantum decoherence, quantifying the departure from a pure state. Indeed, $F_D(t) = 0$ implies that the qubit is in a pure state, while $F_D(t) = 1$ indicates that the qubit is maximally entangled, corresponding to a diagonal density matrix

$$\rho_q = \mathrm{diag}[|c_+|^2, |c_-|^2]. \tag{A8}$$

Notice that the decoherence functions $D(t)$ and $F_D(t)$ do not depend on the spectrum of the qubit Hamiltonian, and in particular on δ.

We also note that, as a consequence of the commutativity between the qubit Hamiltonian H_q and the interaction term H_{qS}, the average qubit energy E_q does not change along the quantum evolution of the global system. Indeed, its value

$$E_q = \langle \Psi(t)|H_q|\Psi(t)\rangle = \mathrm{Tr}[\rho_q H_q] = \sum_{i=\pm} \epsilon_\pm |c_\pm|^2 \tag{A9}$$

remains constant, and therefore it is determined by the initial condition of the qubit.

Since the average total energy must remain constant during the global evolution, Eq. (A9) also implies that

$$E - E_q = \langle \Psi(t)|H_s + H_{qS}|\Psi(t)\rangle \tag{A10}$$

remains constant. Concerning the average work to perform the quench [cf. Eq. (16)], simple calculations lead to

$$\langle W\rangle = \langle \Psi_0|H_{qS}|\Psi_0\rangle = -u(|c_+|^2 - |c_-|^2)\langle 0_h|P|0_h\rangle. \tag{A11}$$

Notice that $\langle W\rangle = 0$, when $|c_+| = |c_-|$.

2. Dynamic FSS at FOQTs for $v = 0$

As discussed in Sec. VI, at FOQTs one may effectively replace the many-body system S with an approximate two-level model such that the composite qubit-system Hamiltonian is written in the matrix form (60). In the specific case $v = 0$, the latter reduces to a block-diagonal form, for which analytic expression can be derived easily.

In practice, the solution of the corresponding Schrödinger problem (61) is still formally given by Eq. (A2). The many-body states $|\Phi_{h\pm u}(\theta)\rangle$ are now replaced by the two-level system states $|\phi_{h\pm u}(\theta)\rangle$, as obtained by solving

$$i\frac{\partial}{\partial \theta}|\phi_{h\pm u}(\theta)\rangle = \hat{H}_{S_2}(h \pm u)|\phi_{h\pm u}(\theta)\rangle, \tag{A12}$$

$$\hat{H}_{S_2}(h \pm u) = H_{S_2}(h \pm u)/\gamma, \tag{A13}$$

with $H_{S_2}(h)$ as in Eq. (55). The initial condition is given by the ground state

$$|\phi_{h\pm u}(\theta=0)\rangle = |0_h\rangle = \sin\left(\frac{\alpha_h}{2}\right)|-\rangle - \cos\left(\frac{\alpha_h}{2}\right)|+\rangle, \tag{A14}$$

with $\tan\alpha_h = \kappa_h^{-1}$ and $\alpha_h \in (0,\pi)$. The quantum evolution described by Eq. (A12) can be easily obtained by diagonalizing the 2×2 Hamiltonian $H_{S_2}(h\pm u)$, whose eigenstates are

$$|0_{h\pm u}\rangle = \sin\left(\frac{\alpha_{h\pm u}}{2}\right)|-\rangle - \cos\left(\frac{\alpha_{h\pm u}}{2}\right)|+\rangle, \tag{A15a}$$

$$|1_{h\pm u}\rangle = \cos\left(\frac{\alpha_{h\pm u}}{2}\right)|-\rangle + \sin\left(\frac{\alpha_{h\pm u}}{2}\right)|+\rangle, \tag{A15b}$$

with $\tan\alpha_{h\pm u} = \kappa_{h\pm u}^{-1}$ and $\alpha_{h\pm u}\in(0,\pi)$. The corresponding energy eigenvalues are

$$E_{0/1} = \Delta(L)\,\mathcal{E}_{0/1}, \quad \mathcal{E}_{0/1} = \mp\tfrac{1}{2}\sqrt{1+\kappa_{h\pm u}^2}. \tag{A16}$$

The time-dependent state evolves as

$$|\phi_{h\pm u}(\theta)\rangle = e^{-i\mathcal{E}_0\theta}\cos\left(\frac{\alpha_h-\alpha_{h\pm u}}{2}\right)|0_{h\pm u}\rangle + e^{-i\mathcal{E}_1\theta}\sin\left(\frac{\alpha_h-\alpha_{h\pm u}}{2}\right)|1_{h\pm u}\rangle. \tag{A17}$$

Then, by rewriting them in terms of the original basis $|\pm\rangle$, using Eqs. (A15), and substituting into Eq. (A2), with $|\phi_{h\pm u}(\theta)\rangle$ instead of $|\Phi_{h\pm u}(\theta)\rangle$, we obtain the solution of the dynamic problem within the two-level approximation of the system S. This reads

$$|\psi(\theta)\rangle = e^{-i(\varepsilon_\delta/2)\theta}c_+|+\rangle\otimes|\phi_{h+u}(\theta)\rangle + e^{+i(\varepsilon_\delta/2)\theta}c_-|-\rangle\otimes|\phi_{h-u}(\theta)\rangle. \tag{A18}$$

This solution is already written in terms of the scaling variables, thus the scaling behaviors put forward in Sec. IV are fully confirmed. The corresponding FSS functions can be analytically computed from their definitions. The scaling function $\mathcal{D}$ associated with the decoherence function D [cf. Eqs. (13) and (38)] is given by

$$\mathcal{D}(\kappa_u,\kappa_h,\theta) = 4|c_+|^2|c_-|^2\kappa_u^2\frac{1-\cos\left(\theta\sqrt{1+\kappa_h^2}\right)}{\left(1+\kappa_h^2\right)^2}. \tag{A19}$$

Arriving at the average work defined in Eq. (16), whose expected scaling behavior is reported in Eq. (48a), we obtain

$$\mathcal{W}_1^{(2l)}(\kappa_u,\kappa_h) = -\frac{1}{2}(|c_+|^2-|c_-|^2)\kappa_u\left[1-2\sin\left(\frac{\alpha_h}{2}\right)^2\right]. \tag{A20}$$

In contrast, for the second moment $\langle W^2\rangle$ we simply obtain

$$\mathcal{W}_2^{(2l)}(\kappa_u,\kappa_h) = \tfrac{1}{4}\kappa_u^2. \tag{A21}$$

For the energy fluctuations of the many-body system S, we may obtain the time dependence of the average energy variation [cf. Eq. (21)] using the formula

$$\mathcal{U}_1^{(2l)}(\theta) = \mathrm{Tr}[\hat{H}_{S_2}(h)\rho(\theta)] - \mathcal{E}_{s0}, \tag{A22}$$

where $\mathcal{E}_{s0} = -\frac{1}{2}\sqrt{1+\kappa_h^2}$. Then, using Eq. (A18), we may write it as

$$\mathcal{U}_1^{(2l)}(\theta) = |c_+|^2\langle\phi_{h+u}(\theta)|\hat{H}_{S_2}(h)|\phi_{h+u}(\theta)\rangle + |c_-|^2\langle\phi_{h-u}(\theta)|\hat{H}_{S_2}(h)|\phi_{h-u}(\theta)\rangle, \tag{A23}$$

where

$$\hat{H}_{S_2}(h) = -\frac{\kappa_h}{2}\sigma^{(3)} + \frac{1}{2}\sigma^{(1)}. \tag{A24}$$

Finally, for the average of the square energy variation we obtain

$$\mathcal{U}_2^{(2l)}(\theta) = \mathrm{Tr}\{[\hat{H}_{S_2}(h)]^2\rho(\theta)\} - 2\mathcal{E}_{s0}\mathcal{U}_1^{(2l)}(\theta) - \mathcal{E}_{s0}^2 = \sqrt{1+\kappa_h^2}\,\mathcal{U}_1^{(2l)}(\theta), \tag{A25}$$

where we used the fact that $[\hat{H}_{S_2}(h)]^2 = (1+\kappa_h^2)I_2$.

APPENDIX B: ACCURACY OF THE TWO-LEVEL APPROXIMATION AT THE FOQT

In Sec. VI B we observed that a two-level reduction of the many-body system to which the qubit is coupled, when the former is at a FOQT, is capable of accurately grasping the asymptotic FSS behavior of several properties of the global system, including the decoherence quantifiers for the qubit and the averages of the work done by the quench and of the energy pumped in the system S. All these quantities are linear functionals of the Hamiltonian H, for which the adiabatic theorem typically applies without any issue [40].

In contrast, Figs. 4 and 7 have spotlighted clear discrepancies when comparing fluctuations of the work and of the system energy (i.e., $\langle W^2\rangle_c$ and $\langle U^2\rangle_c$), with numerically exact diagonalization results for the quantum Ising chains. We believe that such discrepancies are essentially related to the limited accuracy of the two-level approximations, which of course cannot capture the full complexity of a many-body quantum system. Below we provide evidence of this, focusing on a specific quantity. It would be tempting to investigate the problem further, in such a way to achieve a more exhaustive understanding of the accuracy of our approximation. This however lies outside the purposes of this paper and will be left for future work.

Figure 8 compares the time behavior of the system energy and of its square value, evaluated either with the full Hamiltonian H_S or by keeping only its two lowest-energy levels $|\Phi_1\rangle$ and $|\Phi_2\rangle$ (associated with the two energies ε_1 and ε_2), namely, $\langle\Psi(\theta)|H_S|\Psi(\theta)\rangle$ or $\langle\Psi(\theta)|H_S^{(2l)}|\Psi(\theta)\rangle$, respectively, with $H_S^{(2l)} = \varepsilon_1|\Phi_1\rangle + \varepsilon_2|\Phi_2\rangle$. We observe general agreement between the two approaches [Figs. 8(a) and 8(c)]; however, a more detailed analysis reveals that the discrepancies among them are typically one order of magnitude larger for $\langle H_S^2\rangle$ [Fig. 8(b)] than for $\langle H_S\rangle$ [Fig. 8(d)]. Moreover, while the data in Fig. 8(b) suggest that such discrepancies systematically diminish with increasing size, the situation in Fig. 8(d) is less clear and fluctuations at $L=16$ are still quite large. Notice also the appearance of wiggles in Figs. 8(a) and 8(c), concerning the results obtained with a two-level truncation of the Hamiltonian spectrum.

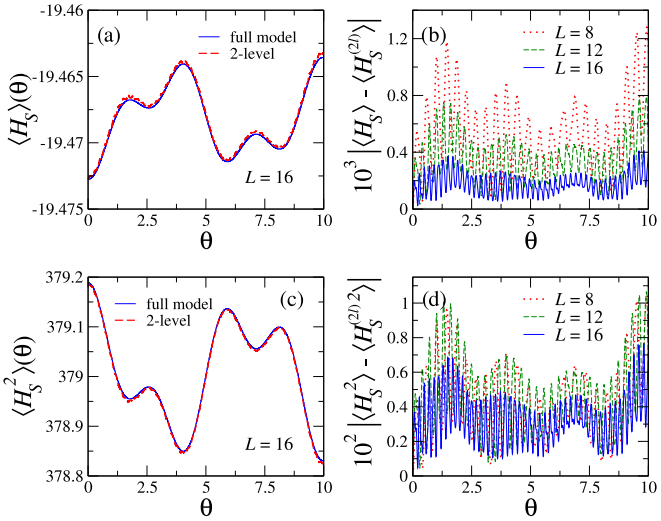

FIG. 8. Comparison of (a) and (b) the average system energy $\langle H_S \rangle$ and (c) and (d) its square value $\langle H_S^2 \rangle$, evaluated using the full many-body Hamiltonian and a truncation to its two lowest levels. The Ising system is at the FOQT with $g = 0.9$, while all the other parameters are set as in Fig. 7. (a) and (c) display the two evolutions, with respect to the rescaled time θ, for a fixed chain length $L = 16$. (b) and (d) highlight the absolute differences between the two cases, for various system sizes.

The discrepancies highlighted above can be amplified when measuring fluctuations. Indeed, in Fig. 9 we show the ratio between the rescaled average energy of the system $\langle U \rangle / \Delta$ and its rescaled fluctuations $\langle U^2 \rangle_c / \Delta^2$. The two-level reduction of system S would predict a value for such a ratio which depends only on κ_h, since it can be shown that Eq. (A25) still holds if $v \neq 0$. In contrast, as displayed in Fig. 9(a), the full simulation shows a nontrivial dependence on θ as well. The comparison between the numerical values averaged over θ (horizontal dashed lines) and the analytic estimate $\sim 1/\sqrt{1+\kappa_h^2}$ given by Eq. (A25) is provided in Fig. 9(b), as a function of κ_h. Similarly to what was observed in Figs. 6(b) and 7(b), we highlight the emergence of a discrepancy between the two approaches, which however cannot be interpreted as a simple offset independent of the value of κ_h.

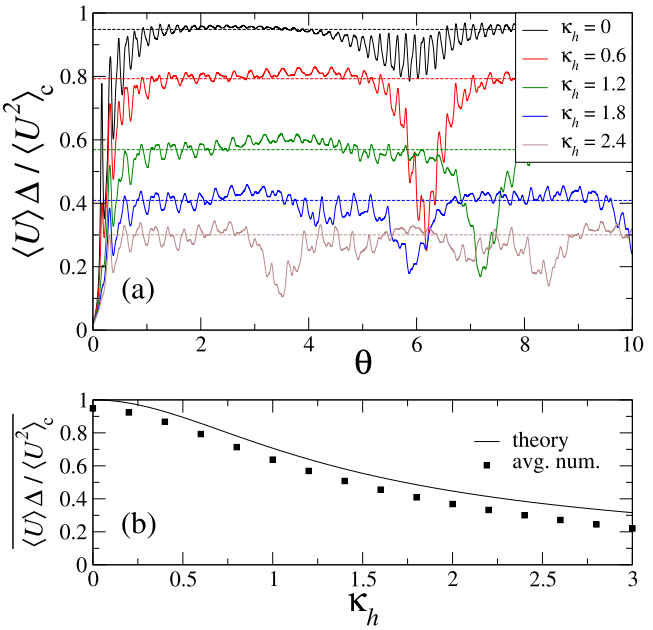

FIG. 9. (a) Ratio between the rescaled average energy of the system and its rescaled fluctuations, as a function of θ. The various curves are for different values of κ_h, as indicated in the legend (from top to bottom, curves are for increasing κ_h). (b) Comparison between numerical data averaged over the time [see the horizontal dashed lines in (a)] and the analytic estimate $\mathcal{U}_1/\mathcal{U}_2 = 1/\sqrt{1+\kappa_h^2}$, as given by Eq. (A25). Data are for an Ising-chain system with $L = 12$ sites, while all the other parameters are set as in Fig. 8.

[1] J. Dziarmaga, Dynamics of a quantum phase transition and relaxation to a steady state, Adv. Phys. **59**, 1063 (2010).

[2] A. Polkovnikov, K. Sengupta, A. Silva, and M. Vengalattore, Colloquium: Nonequilibrium dynamics of closed interacting quantum systems, Rev. Mod. Phys. **83**, 863 (2011).

[3] R. Nandkishore and D. A. Huse, Many body localization and thermalization in quantum statistical mechanics, Annu. Rev. Condens. Matter Phys. **6**, 15 (2015).

[4] T. Kinoshita, T. Wenger, and D. S. Weiss, A quantum Newton's cradle, Nature (London) **440**, 900 (2006).

[5] S. Hofferberth, I. Lesanovsky, B. Fischer, T. Schumm, and J. Schmiedmayer, Non-equilibrium coherence dynamics in one-dimensional Bose gases, Nature (London) **449**, 324 (2007).

[6] S. Trotzky, Y.-A. Chen, A. Flesch, I. P. McCulloch, U. Schollwöck, J. Eisert, and I. Bloch, Probing the relaxation towards equilibrium in an isolated strongly correlated one-dimensional Bose gas, Nat. Phys. **8**, 325 (2012).

[7] M. Cheneau, P. Barmettler, D. Poletti, M. Endres, P. Schauß, T. Fukuhara, C. Gross, I. Bloch, C. Kollath, and S. Kuhr, Light-cone-like spreading of correlations in a quantum many-body system, Nature (London) **481**, 484 (2012).

[8] M. Schreiber, S. S. Hodgman, P. Bordia, H. P. Lüschen, M. H. Fischer, R. Vosk, E. Altman, U. Schneider, and I. Bloch, Observation of many-body localization of interacting fermions in a quasirandom optical lattice, Science **349**, 842 (2015).

[9] A. M. Kaufman, M. E. Tai, A. Lukin, M. Rispoli, R. Schittko, P. M. Preiss, and M. Greiner, Quantum thermalization through entanglement in an isolated many-body system, Science **353**, 794 (2016).

[10] J. Smith, A. Lee, P. Richerme, B. Neyenhuis, P. W. Hess, P. Hauke, M. Heyl, D. A. Huse, and C. Monroe, Many-body localization in a quantum simulator with programmable random disorder, Nat. Phys. **12**, 907 (2016).

[11] C. Maier, T. Brydges, P. Jurcevic, N. Trautmann, C. Hempel, B. P. Lanyon, P. Hauke, R. Blatt, and C. F. Roos, Environment-Assisted Quantum Transport in a 10-qubit Network, Phys. Rev. Lett. **122**, 050501 (2019).

[12] M. Esposito, U. Harbola, and S. Mukamel, Nonequilibrium fluctuations, fluctuation theorems, and counting statistics in quantum systems, Rev. Mod. Phys. **81**, 1665 (2009).

[13] C. Jarzynski, Equalities and inequalities: Irreversibility and the second law of thermodynamics at the nanoscale, Annu. Rev. Condens. Matter Phys. **2**, 329 (2011).

[14] M. Campisi, P. Hänggi, and P. Talkner, Colloquium: Quantum fluctuation relations: Foundations and applications, Rev. Mod. Phys. **83**, 771 (2011).

[15] U. Seifert, Stochastic thermodynamics, fluctuation theorems and molecular machines, Rep. Prog. Phys. **75**, 126001 (2012).

[16] W. H. Zurek, Decoherence, einselection, and the quantum origins of the classical, Rev. Mod. Phys. **75**, 715 (2003).

[17] F. Caruso, A. W. Chin, A. Datta, S. F. Huelga, and M. B. Plenio, Highly efficient energy excitation transfer in light-harvesting complexes: The fundamental role of noise-assisted transport, J. Chem. Phys. **131**, 105106 (2009).

[18] N. Lambert, Y.-N. Chen, Y.-C. Cheng, C.-M. Li, G.-Y. Chen, and F. Nori, Quantum biology, Nat. Phys. **9**, 10 (2013).

[19] F. C. Binder, S. Vinjanampathy, K. Modi, and J. Goold, Quantacell: Powerful charging of quantum batteries, New J. Phys. **17**, 075015 (2015).

[20] F. Campaioli, F. A. Pollock, F. C. Binder, L. Céleri, J. Goold, S. Vinjanampathy, and K. Modi, Enhancing the Charging Power of Quantum Batteries, Phys. Rev. Lett. **118**, 150601 (2017).

[21] T. P. Le, J. Levinsen, K. Modi, M. M. Parish, and F. A. Pollock, Spin-chain model of a many-body quantum battery, Phys. Rev. A **97**, 022106 (2018).

[22] D. Ferraro, M. Campisi, G. M. Andolina, V. Pellegrini, and M. Polini, High-Power Collective Charging of a Solid-State Quantum Battery, Phys. Rev. Lett. **120**, 117702 (2018).

[23] S. Julia-Farre, T. Salamon, A. Riera, M. N. Bera, and M. Lewenstein, Bounds on capacity and power of quantum batteries, arXiv:1811.04005.

[24] S. Sachdev, *Quantum Phase Transitions* (Cambridge University, Cambridge, 1999).

[25] W. H. Zurek, Environment-induced superselection rules, Phys. Rev. D **26**, 1862 (1982).

[26] F. M. Cucchietti, J. P. Paz, and W. H. Zurek, Decoherence from spin environments, Phys. Rev. A **72**, 052113 (2005).

[27] H. T. Quan, Z. Song, X. F. Liu, P. Zanardi, and C. P. Sun, Decay of Loschmidt Echo Enhanced by Quantum Criticality, Phys. Rev. Lett. **96**, 140604 (2006).

[28] D. Rossini, T. Calarco, V. Giovannetti, S. Montangero, and R. Fazio, Decoherence induced by interacting quantum spin baths, Phys. Rev. A **75**, 032333 (2007).

[29] F. M. Cucchietti, S. Fernandez-Vidal, and J. P. Paz, Universal decoherence induced by an environmental quantum phase transition, Phys. Rev. A **75**, 032337 (2007).

[30] C. Cormick and J. P. Paz, Decoherence induced by a dynamic spin environment: The universal regime, Phys. Rev. A **77**, 022317 (2008).

[31] W. H. Zurek, Quantum Darwinism, Nat. Phys. **5**, 181 (2009).

[32] B. Damski, H. T. Quan, and W. H. Zurek, Critical dynamics of decoherence, Phys. Rev. A **83**, 062104 (2011).

[33] T. Nag, U. Divakaran, and A. Dutta, Scaling of the decoherence factor of a qubit coupled to a spin chain driven across quantum critical points, Phys. Rev. B **86**, 020401(R) (2012).

[34] S. Suzuki, T. Nag, and A. Dutta, Dynamics of decoherence: Universal scaling of the decoherence factor, Phys. Rev. A **93**, 012112 (2016).

[35] E. Vicari, Decoherence dynamics of qubits coupled to systems at quantum transitions, Phys. Rev. A **98**, 052127 (2018).

[36] E. Fiorelli, A. Cuccoli, and P. Verrucchi, Critical slowing down and entanglement protection, arXiv:1901.07985.

[37] M. Campostrini, A. Pelissetto, and E. Vicari, Finite-size scaling at quantum transitions, Phys. Rev. B **89**, 094516 (2014).

[38] M. Campostrini, J. Nespolo, A. Pelissetto, and E. Vicari, Finite-Size Scaling at First-Order Quantum Transitions, Phys. Rev. Lett. **113**, 070402 (2014).

[39] A. Pelissetto, D. Rossini, and E. Vicari, Dynamic finite-size scaling after a quench at quantum transitions, Phys. Rev. E **97**, 052148 (2018).

[40] A. Pelissetto, D. Rossini, and E. Vicari, Out-of-equilibrium dynamics driven by localized time-dependent perturbations at quantum phase transitions, Phys. Rev. B **97**, 094414 (2018).

[41] J. Zinn-Justin, *Quantum Field Theory and Critical Phenomena*, fourth edition (Clarendon, Oxford, 2002).

[42] A. Pelissetto and E. Vicari, Critical phenomena and renormalization-group theory, Phys. Rep. **368**, 549 (2002).

[43] J. Goold, F. Plastina, A. Gambassi, and A. Silva, in *Thermodynamics in the Quantum Regime: Fundamental aspects and new directions*, edited by F. Binder, L. A. Correa, C. Gogolin, J. Anders, and G. Adesso, Fundamental Theories of Physics Vol. 195 (Springer International, Cham, 2018).

[44] P. Talkner and P. Hänggi, Aspects of quantum work, Phys. Rev. E **93**, 022131 (2016).

[45] P. Talkner, E. Lutz, and P. Hänggi, Fluctuation theorems: Work is not an observable, Phys. Rev. E **75**, 050102(R) (2007).

[46] D. Nigro, D. Rossini, and E. Vicari, Scaling properties of work fluctuations after quenches near quantum transitions, J. Stat. Mech. (2019) 023104.

[47] M. Campostrini, J. Nespolo, A. Pelissetto, and E. Vicari, Finite-size scaling at first-order quantum transitions of quantum Potts chains, Phys. Rev. E **91**, 052103 (2015).

[48] A. Pelissetto, D. Rossini, and E. Vicari, Finite-size scaling at first-order quantum transitions when boundary conditions favor one of the two phases, Phys. Rev. E **98**, 032124 (2018).

[49] M. Campostrini, A. Pelissetto, and E. Vicari, Quantum transitions driven by one-bond defects in quantum Ising rings, Phys. Rev. E **91**, 042123 (2015); Quantum Ising chains with boundary fields, J. Stat. Mech. (2015) P11015.

[50] D. Rossini and E. Vicari, Ground-state fidelity at first-order quantum transitions, Phys. Rev. E **98**, 062137 (2018).

[51] P. Pfeuty, The one-dimensional Ising model with a transverse field, Ann. Phys. (NY) **57**, 79 (1970).

[52] V. Privman and M. E. Fisher, Finite-size effects at first-order transitions, J. Stat. Phys. **33**, 385 (1983).

[53] G. G. Cabrera and R. Jullien, Universality of Finite-Size Scaling: Role of the Boundary Conditions, Phys. Rev. Lett. **57**, 393 (1986); Role of the boundary conditions in the finite-size Ising model, Phys. Rev. B **35**, 7062 (1987).

[54] M. N. Barber, in *Phase Transitions and Critical Phenomena*, edited by C. Domb and J. L. Lebowitz (Academic, London 1983), Vol. 8, p. 145.

[55] *Finite Size Scaling and Numerical Simulations of Statistical Systems*, edited by V. Privman (World Scientific, Singapore, 1990).

[56] R. Guida and J. Zinn-Justin, Critical exponents of the ***N***-vector model, J. Phys. A: Math. Gen. **31**, 8103 (1998).

[57] M. Campostrini, A. Pelissetto, P. Rossi, and E. Vicari, 25th-order high-temperature expansion results for three-dimensional Ising-like systems on the simple-cubic lattice, Phys. Rev. E **65**, 066127 (2002).

[58] M. Hasenbusch, Finite size scaling study of lattice models in the three-dimensional Ising universality class, Phys. Rev. B **82**, 174433 (2010).

[59] F. Kos, D. Poland, D. Simmons-Duffin, and A. Vichi, Precision islands in the Ising and $O(N)$ models, J. High Energy Phys. 08 (2016) 036.

[60] M. V. Kompaniets and E. Panzer, Minimally subtracted six-loop renormalization of $O(n)$-symmetric φ^4 theory and critical exponents, Phys. Rev. D **96**, 036016 (2017).

[61] T. Gorin, T. Prosen, T. H. Seligman, and M. Žnidarič, Dynamics of Loschmidt echoes and fidelity decay, Phys. Rep. **435**, 33 (2006).

[62] L. Amico, R. Fazio, A. Osterloh, and V. Vedral, Entanglement in many-body systems, Rev. Mod. Phys. **80**, 517 (2008).

[63] S.-J. Gu, Fidelity approach to quantum phase transitions, Int. J. Mod. Phys. B **24**, 4371 (2010).

[64] D. Braun, G. Adesso, F. Benatti, R. Floreanini, U. Marzolino, M. W. Mitchell, and S. Pirandola, Quantum-enhanced measurements without entanglement, Rev. Mod. Phys. **90**, 035006 (2018).

[65] G. De Chiara and A. Sanpera, Genuine quantum correlations in quantum many-body systems: A review of recent progress, Rep. Prog. Phys. **81**, 074002 (2018).

[66] J. Simon, W. S. Bakr, R. Ma, M. E. Tai, P. M. Preiss, and M. Greiner, Quantum simulation of antiferromagnetic spin chains in an optical lattice, Nature (London) **472**, 307 (2011).

[67] E. E. Edwards, S. Korenblit, K. Kim, R. Islam, M.-S. Chang, J. K. Freericks, G.-D. Lin, L.-M. Duan, and C. Monroe, Quantum simulation and phase diagram of the transverse-field Ising model with three atomic spins, Phys. Rev. B **82**, 060412(R) (2010).

[68] R. Islam, E. E. Edwards, K. Kim, S. Korenblit, C. Noh, H. Carmichael, G.-D. Lin, L.-M. Duan, C.-C. Joseph Wang, J. K. Freericks, and C. Monroe, Onset of a quantum phase transition with a trapped ion quantum simulator, Nat. Commun. **2**, 377 (2011).

[69] G.-D. Lin, C. Monroe, and L.-M. Duan, Sharp Phase Transitions in a Small Frustrated Network of Trapped Ion Spins, Phys. Rev. Lett. **106**, 230402 (2011).

[70] K. Kim, S. Korenblit, R. Islam, E. E. Edwards, M.-S. Chang, C. Noh, H. Carmichael, G.-D. Lin, L.-M. Duan, C. C. Joseph Wang, J. K. Freericks, and C. Monroe, Quantum simulation of the transverse Ising model with trapped ions, New J. Phys. **13**, 105003 (2011).

[71] S. Debnath, N. M. Linke, C. Figgatt, K. A. Landsman, K. Wright, and C. Monroe, Demonstration of a small programmable quantum computer with atomic qubits, Nature (London) **536**, 63 (2016).

[72] H. Labuhn, D. Barredo, S. Ravets, S. de Leseleuc, T. Macri, T. Lahaye, and A. Browaeys, Tunable two-dimensional arrays of single Rydberg atoms for realizing quantum Ising models, Nature (London) **534**, 667 (2016).